



Article

Assessment of Vegetation Dynamics and Ecosystem Resilience in the Context of Climate Change and Drought in the Horn of Africa

Simon Measho ^{1,2,3} , Baozhang Chen ^{1,2,4,5,*} , Petri Pellikka ^{6,7} , Lifeng Guo ^{1,2}, Huifang Zhang ^{1,2}, Diwen Cai ⁸ , Shaobo Sun ⁹ , Alphonse Kayiranga ^{1,2}, Xiaohong Sun ¹⁰ and Mengyu Ge ⁴

- ¹ State Key Laboratory of Resources and Environment Information System, Institute of Geographic Sciences and Natural Resources Research, Chinese Academy of Sciences, 11A, Datun Road, Chaoyang District, Beijing 100101, China; simon@igsnr.ac.cn (S.M.); guolf.15b@igsnr.ac.cn (L.G.); zhanghf@igsnr.ac.cn (H.Z.); akayiranga2018@igsnr.ac.cn (A.K.)
- ² University of Chinese Academy of Sciences, No. 19A, Yuquan Road, Beijing 100049, China
- ³ Department of Land Resources and Environment, Hamelmalo Agricultural College, Keren 397, Eritrea
- ⁴ School of Remote Sensing and Geomatics Engineering, Nanjing University of Information Science and Technology, Nanjing 210044, China; mengyu.ge@helsinki.fi
- ⁵ Jiangsu Center for Collaborative Innovation in Geographical Information Resource Development and Application, Nanjing 210023, China
- ⁶ Earth Change Observation Laboratory, Department of Geosciences and Geography, University of Helsinki, 00100 Helsinki, Finland; petri.pellikka@helsinki.fi
- ⁷ State Key Laboratory for Information Engineering in Surveying, Mapping and Remote Sensing, Wuhan University, Wuhan 430079, China
- ⁸ Key Laboratory of Water Cycle and Related Land Surface Processes, Institute of Geographic Sciences and Natural Resources Research, Chinese Academy of Sciences, Beijing 100101, China; caidw.17b@igsnr.ac.cn
- ⁹ Institute of Surface-Earth System Science, School of Earth System Science, Tianjin University, Tianjin 300072, China; shaobo.sun@tju.edu.cn
- ¹⁰ Key Laboratory for Water and Sediment Science, College of Environmental Sciences and Engineering, Peking University, Beijing 100871, China; xh.sun@pku.edu.cn
- * Correspondence: baozhang.chen@igsnr.ac.cn



Citation: Measho, S.; Chen, B.; Pellikka, P.; Guo, L.; Zhang, H.; Cai, D.; Sun, S.; Kayiranga, A.; Sun, X.; Ge, M. Assessment of Vegetation Dynamics and Ecosystem Resilience in the Context of Climate Change and Drought in the Horn of Africa. *Remote Sens.* **2021**, *13*, 1668. <https://doi.org/10.3390/rs13091668>

Academic Editors: Javier J. Cancela and Magaly Koch

Received: 10 February 2021

Accepted: 21 April 2021

Published: 25 April 2021

Publisher's Note: MDPI stays neutral with regard to jurisdictional claims in published maps and institutional affiliations.



Copyright: © 2021 by the authors. Licensee MDPI, Basel, Switzerland. This article is an open access article distributed under the terms and conditions of the Creative Commons Attribution (CC BY) license (<https://creativecommons.org/licenses/by/4.0/>).

Abstract: Understanding the response of vegetation and ecosystem resilience to climate variability and drought conditions is essential for ecosystem planning and management. In this study, we assessed the vegetation changes and ecosystem resilience in the Horn of Africa (HOA) since 2000 and detected their drivers based mainly on analysis of the Moderate Resolution Imaging Spectroradiometer (MODIS) products. We found that the annual and seasonal trends of NDVI (Normalized Difference Vegetation Index) generally increased during the last two decades over the Horn of Africa particularly in western parts of Ethiopia and Kenya. The weakest annual and seasonal NDVI trends were observed over the grassland cover and tropical arid agroecological zones. The NDVI variation negatively correlated with Land Surface Temperature (LST) and positively correlated with precipitation at a significant level ($p < 0.05$) account for 683,197 km² and 533,385 km² area, respectively. The ecosystem Water Use Efficiency (eWUE) showed overall increasing trends with larger values for the grassland biome. The precipitation had the most significant effect on eWUE variation compared to LST and annual SPEI (Standardized Evapotranspiration Index). There were about 54.9% of HOA resilient to drought disturbance, whereas 32.6% was completely not-resilient. The ecosystems in the humid agroecological zones, the cropland, and wetland were slightly not-resilient to severe drought conditions in the region. This study provides useful information for policy makers regarding ecosystem and dryland management in the context of climate change at both national and regional levels.

Keywords: vegetation dynamics; ecosystem resilience; MODIS NDVI; water use efficiency; climate change; climate variability; drought; precipitation; LST; SPEI

1. Introduction

The Horn of Africa has been affected by its location in the tropics under the influence of the Sahara and Arabian Desert, the Red Sea, and the Indian Ocean. Climate variability in the region is certain [1], and there is a high rate of vulnerability to the impacts of climate change in the plant species and the people who depend on the rain-fed farming [2]. Climate variability across East Africa from historical records show that temperatures have increased by 1.5–2 °C on average and there are large rainfall variations in the direction and magnitude of changes over the past 50 years [3]. The countries in the Horn of Africa have been exposed to series of drought, and the region at large is exposed to the effects of drought, and the causes are associated with climate change and climate variability [4]. Land surface temperature shows an increasing pattern in many countries of the Horn of Africa, for instance, Abera et al. [5] identified an increase of the annual average land surface temperature as high as 1.8 °C in Ethiopia. Consequently, the overall impact of climate variability and climate change on vegetation dynamics and pressure on ecosystem services has been immense especially during the last two decades.

The biodiversity of the Horn of Africa is also threatened due to land cover and land use changes mainly caused by deforestation. A recent study of land use/land covers changes in the Horn of Africa confirms that forested areas were decreased and there was an expansion in built-up areas (2000–2015) with large impacts on water yield and latent effect to ecosystem services [6]. Specific biodiversity analysis in tropical Africa indicates that 33% of the plant species are potentially threatened with extinction, while Ethiopia is one of the four highlighted regions with a high percentage of potentially threatened species [7]. Similarly, a recent study on land use/land cover change on ecosystem services in the central highlands of Ethiopia [8], concluded that forest cover was reduced by 54.2% from 1973 to 2015 with a very large loss in ecosystem service values. Loss of forest cover or even bushlands lead to decreased carbon sequestration by the woody vegetation [9] and increased land surface temperature and evapotranspiration [10] as shown in Southern Kenya, thus causing climate change first in a small area and, when it happens through the region, then largely. Ecosystem change detections are limited by uncertainties in climate change predictions and their driving forces [11]. The assessment of plant conditions and vegetation dynamics with the impacts of drought and climate variability can be essential to understand the changes in the terrestrial ecosystem and ecosystem resilience to different disturbances.

Vegetation dynamics may cause variations in the phenology and changes in the performance of plant species at different time scales [12]. Studies on vegetation dynamics and their quantification are numerous, and accurate measurement at larger areas may increase human understanding of the dynamics in the terrestrial ecosystem, carbon exchange system, and climate-biosphere interactions in the environment [13,14]. The dynamics of vegetation for small areas can be assessed and monitored with field-based measurements [15], however, as the spatial coverage and temporal variability increases, the complexity of the vegetation and types in structure and phenology also changes and varies essentially.

The use of satellite imaging has increased and become a key tool for ecological scientists to monitor seasonal and inter-annual vegetation dynamics [16]. Hence, the use of remote sensing products such as normalized difference vegetation index (NDVI), leaf area index (LAI), gross primary productivity (GPP), and evapotranspiration (ET) become feasible to analyze the trend and productivity of vegetation as well as to evaluate the ecosystem water use efficiency (eWUE) and ecosystem resilience. Time series of NDVI and LAI can provide very valuable information about changes in the terrestrial ecosystem and specifically detect trends in the vegetation dynamics and phenology [17]. The assessment of eWUE based on GPP and ET in addition to NDVI variations can be essential to understand the ecosystem carbon-water coupling under climate change in the region [18], and this may further increase the information to predict vegetation growth, ecosystem resilience analysis, and ecosystem management [19].

The vegetation dynamics studies in the African continent are focused more on the Sahel region and only a few are found in East Africa with a limited extent to the Horn of Africa. For instance, a study on trends of vegetation dynamics for the African Sahel showed positive greening trends in NDVI and a net increase in biomass production between 1982 and 2003 [20]. Although the reasons are largely attributed to rainfall variations, further analysis based on higher resolutions from MODIS and LANDSAT is recommended. A recent study on ecohydrological resilience for the whole of Africa using coarse spatial resolutions identified 31.22% of the terrestrial ecosystems being non-resilient to ecosystem shifts [21]. In East Africa, the vegetation dynamics based on LAI assessment between 1982 and 2011 showed LAI increased in the region at a rate of about 4×10^{-3} units per year and it is believed the trend encountered series of breaks and variations [22]. Conversely, in the same period between 1982 and 2011, vegetation trend estimates based on LAI in Eastern Africa demonstrated a persistent decrease in areas from Southern Ethiopia through central Kenya to central Tanzania [23]. Moreover, Kalisa et al. [24] found a positive linear trend between 1981 and 1998, while there was a negative linear trend during 1998–2015 over East Africa using the NDVI3g dataset. Likewise, Ghebregabher et al. [25] assessed vegetation variations in the Horn of Africa based on GIMMS data and concluded that the mean NDVI slowly decreased from 1998 to 2013.

This research aims to provide a detailed and higher spatial resolution assessment in the vegetation dynamics and ecosystem resilience analysis to climate variables (precipitation and land surface temperature), and the drought factor, considering the limited focus of such study in the region. The improved outputs can supply up-to-date regional spatial information for ecosystem management and planning. There are gaps and disagreement in research findings related to the vegetation trends in East Africa, and a lack of ecosystem resilience study to drought which is the main natural hazard in the region. Moreover, most of the vegetation dynamics studies in the Horn of Africa give less attention to interpretation based on agroecological zones, and it has not been possible to quantify ecosystem water use efficiency in the region. Therefore, the specific objectives of this study are three-fold: (i) To analyze the annual and seasonal MODIS NDVI trends in the last two decades; (ii) to find the main causes of vegetation change and water use efficiency variations based on main climate variables; and (iii) to assess ecosystem water use efficiency and ecosystem resilience to drought in the Horn of Africa.

2. Materials and Methods

2.1. Study Area

The study area covers the Horn of Africa (HoA), which includes Eritrea, Ethiopia, Djibouti, Somalia, and Kenya (Figure 1). The Horn of Africa is one of the highest populated regions of Africa, and the total population reaches about 165 million, of which Ethiopia is the most populous country. The region encompasses diversified mountains, highlands, valleys, plains, and lowlands. The topography of the region descends from about 5200 meters above mean sea level at Mt. Kenya to about 126 meters below sea level in the Danakil Depression at the border area of Eritrea and Ethiopia (Figure 1).

The climate of the Horn of Africa is characterized by warm arid in the coastal areas and lowlands of Somalia, Djibouti, and Eritrea, warm semi-arid in the lowlands of Ethiopia and Kenya, cool humid in the high mountains of Ethiopia and Kenya, warm, humid climate dominating highlands of Ethiopia and Kenya, while Western Kenya is hot and humid. The climate variability in the region is highly influenced by the movement of the Intertropical Convergence Zone (ITCZ), the effect of the Sahara Desert, especially in the northeastern parts, El Niño Southern Oscillation (ENSO), and the warm Indian Ocean currents and surface temperature changes [1,26,27]. Bimodal seasonal rainfall distributions characterize Horn of Africa [28]; according to 2001–2016 Tropical Rainfall Measuring Mission (TRMM) data, the mean annual precipitation ranges from 81 to 2130 mm in the lowlands per year in the highlands [29]. The main rainfall regimes and seasons of the Horn of Africa are wet from March to May, dry from June to August, wet from September to November, and

dry from December to February, but there are obvious differences from southern Kenya to Eritrea with this seasonality.

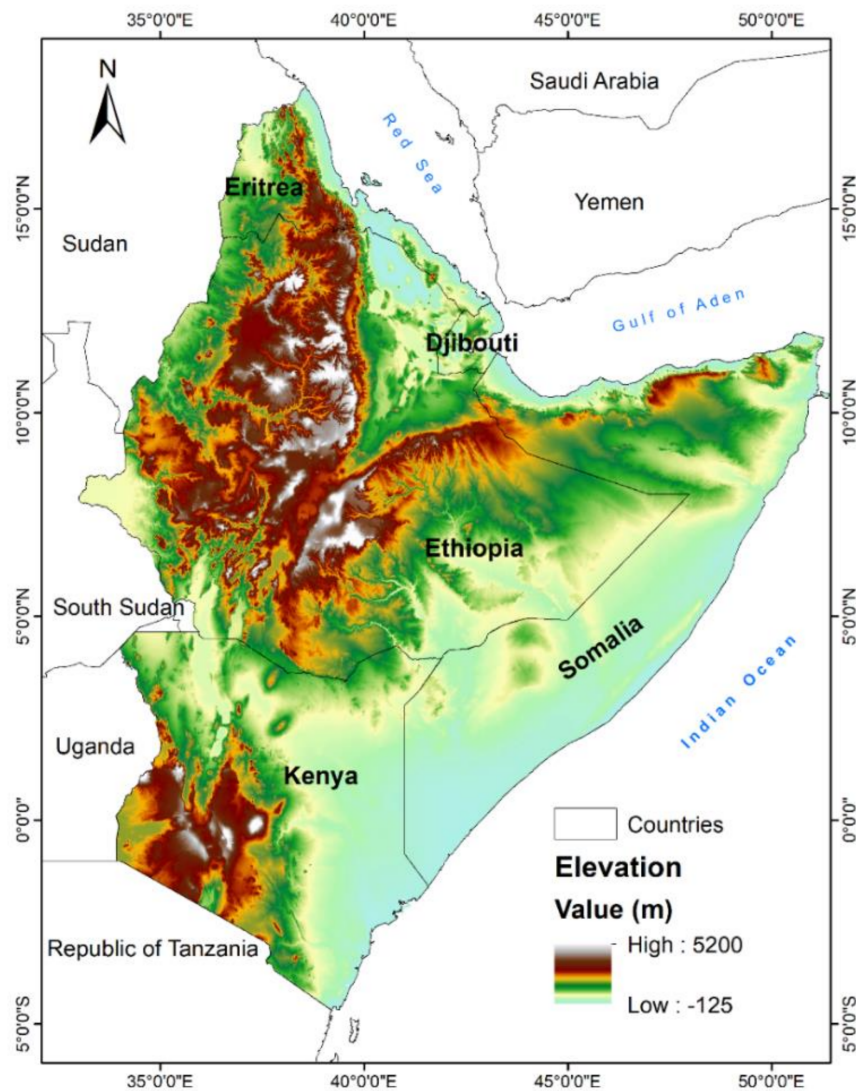


Figure 1. The elevation range in the Horn of Africa (DEM source: SRTM) and the countries within.

The land cover can be generalized from the satellite image extractions. The European Space Agency land use/land cover data (2015) of 300 m spatial resolution shows that the most dominant land covers are shrublands, croplands (agriculture), forest areas, and grasslands representing 38.9%, 20.4%, 14.1%, and 12.6%, respectively (Figure 2a). Grasslands and shrublands are dominant in southern parts of Ethiopia and Somalia, and northern parts of Kenya. Cropland land occupies large parts of the highland areas of Kenya, Ethiopia, and Eritrea. Agricultural activities, forests, and water bodies are more common in the western parts of the Horn of Africa and in the Rift Valley areas [30]. The most dominant agroecological zones in the Horn of Africa are of tropical climatic types which include warm arid, warm semi-arid, cool semi-humid, and cool semi-arid types covering 36.3%, 19.6%, 2.5%, and 1.2%, respectively (Figure 2b). The tropical warm arid zones are common in large parts of Somalia and Djibouti, western and eastern lowlands of Eritrea, and the eastern side of Kenya. Apart from the impact of climate change on terrestrial vegetation production and phenology, clearing forests and shrublands for the agricultural purpose by farmers is a common practice in some countries of the region, and this has increased the pressure on the land and endangered ecosystem services [31].

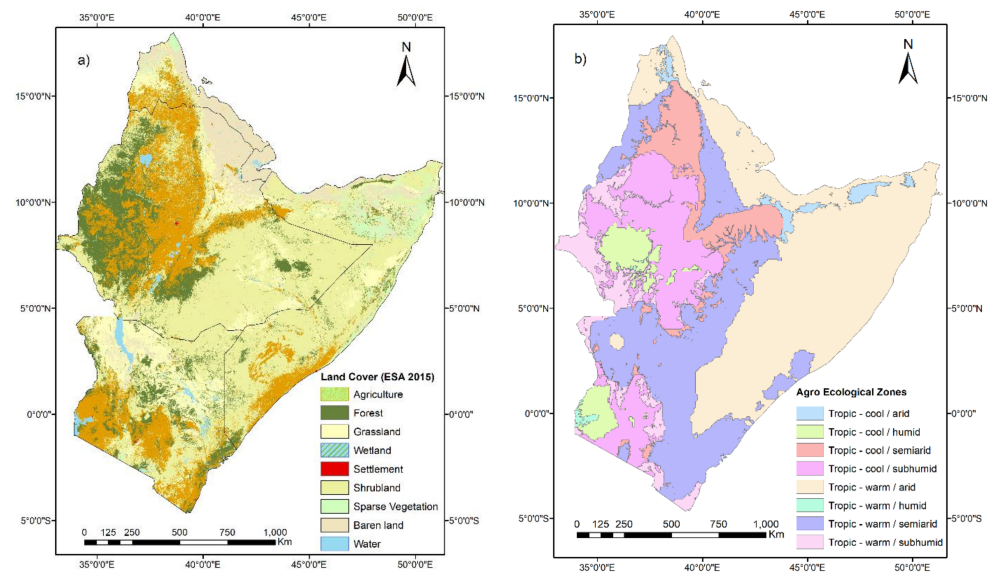


Figure 2. Land cover types (a) and agroecological zones (b) in the Horn of Africa. Data source: ESA land cover 2015, and RCMRD GeoPortal for the Agroecological zones.

2.2. Data

We applied and reprocessed different raster and vector datasets to assess the vegetation dynamics and ecosystem resilience in the Horn of Africa. Time series images of NDVI Terra 16-day of MODIS13Q1 version 6 at 250 m spatial resolution and Land Surface Temperature (LST) of MODIS Terra 8-day at 1km from MODIS dataset of LPDAAC NASA Products, and CHIRPS daily gridded precipitation at 0.05° from CHIRPS dataset were all accessed and retrieved from Climate Engine (<https://app.climateengine.org/climateEngine>) for the last 20 years. The Climate Engine provides both climate, hydrology, and remote sensing related products in an easily accessible spatial format, spatially filtered datasets, and it minimized computational barriers through Google Earth's cloud computing methods [32,33].

We utilized existing time series Global GPP and ET images of high spatial resolutions (0.0083°) as annual MOD17A3 and MOD16A3 products prepared by the Numerical Terra-dynamic Simulation Group from the NASA MODIS outputs at the University of Montana (http://files.ntsg.umt.edu/data/NTSG_Products/). These satellite images cover 15 years since 2000 are used to estimate the ecosystem water use efficiency and compute the ecosystem resilience in the Horn of Africa. The global daily GPP and annual ET of the MODIS products were applied in previous research works [19,34,35]. The MOD17 images for the global GPP exclude areas of no or limited vegetation cover, and the images were initially validated using class C 0.5° of the Ecosystem Model-Data Intercomparison as a base dataset [35]. High-resolution SPEI-12 dataset (0.05°) from CEDA Archive of the Natural Environment Research Council's Data Repository (<https://catalogue.ceda.ac.uk/>) was further processed and used to detect the trend and correlation analysis of the drought in recent years, and used to identify the most severe drought year to be considered for the ecosystem resilience analysis.

Other ancillary data used in this study include Digital Elevation Model (DEM), Land Cover, and Agroecological Zones. The DEM was extracted from the USGS SRTM data center prepared by CGIAR-CSI (<http://srtm.csi.cgiar>), and it has close to 30 m spatial resolution near the Equator. The European Space Agency (ESA) land cover product of 300 m for the year 2015 was extracted from CCI-LC (Climate Change Initiative-Land Cover) project which prepares reliable Global LC maps from 1992 to 2015 with 31 land cover classes (<ftp://geo10.elie.ucl.ac.be/v207/>). We reclassified the land cover product into nine major classes using the land cover CCI Product user guide, version 2. The latest CCI-LC products show a higher potential for cropland monitoring and can provide a good base for general classification [36]. The agroecological zones shapefile for Africa was accessed from RCMRD

GeoPortal (<http://geoportal.rcmr.org/>) using the Food and Agricultural Organization of the United Nations (FAO) methodology (2009), RCMRD provides geospatial datasets especially for the Eastern and Southern Africa region. The agroecological zones shapefile was masked to the area of Interest.

2.3. Methods

2.3.1. Trend Detection

A pixel based linear trend was used to assess the temporal variations of vegetation change. The slope was determined by linear regression which detects the mean annual and seasonal changes in MODIS NDVI either as increasing or decreasing trend during 2000–2019. The trend in the vegetation at each pixel was calculated as given in Equation 1:

$$Slope = \frac{n \times \sum_{i=1}^n X_i Y_i - \sum_{i=1}^n X_i \sum_{i=1}^n Y_i}{n \times \sum_{i=1}^n X_i^2 - (\sum_{i=1}^n X_i)^2} \quad (1)$$

where *Slope* stands for the changing trends in the annual MODIS NDVI, and *n* is the number of the samples (20 years). *X_i* is the time as an independent variable and *Y_i* is the dependent variable (NDVI), both represent the *i*th year in the time series.

The significance of the trend was detected by applying the non-parametric statistical method of Mann–Kendal. Thus, the existence of a monotonic increase or decrease in the temporal trend was tested using the Mann–Kendal with normalized statistics (*Z*). The test of the normal distribution (*Z*) is determined from the Mann–Kendell statistics (*S*) and its variance as described by different authors [37–39]. In the time series MODIS NDVI images, all pixel values less than 0.1 were masked out to reduce the effect of barren and limited land cover reflections for the vegetation trend analysis and results.

2.3.2. Correlation Analysis

To depict the main climatic factors which control the vegetation dynamics and in the Horn of Africa during the period 2000–2019, correlation analysis between NDVI and climate variables such as precipitation and LST was computed. Similarly, the Pearson correlation analysis between annual eWUE and SPEI was performed at the pixel level to incorporate other climatic factors and observe the difference in vegetation production changes due to drought. We used an upscaled 16-day MODIS Terra NDVI and MODIS LST at a 1 km spatial resolution from the Climate Engine, and resampled the CHIRPS daily gridded precipitation at a 5 km resolution using bilinear resampling method to match the NDVI and LST grids. Further, we resampled the SPEI with a 0.05° resolution, LST and precipitation data to the spatial resolution of the MODIS GPP and ET at a 0.0083° (~921 m) resolution. The *r* was computed in Equation 2 following the approach [40,41]:

$$r_{xy} = \frac{\sum_{i=1}^n [(x_i - X)(y_i - Y)]}{\sqrt{\sum_{i=1}^n (x_i - X)^2 \sum_{i=1}^n (y_i - Y)^2}} \quad (2)$$

where *r_{xy}* is the correlation between *X* and *Y* variables, *y_i* refers to NDVI in the *i*th year, and *x_i* represents the climate (precipitation or LST) of the *i*th year; *Y* is the total mean NDVI value for the 20 years, and *X* is the total average climate value for the study period. The *r* was tested using F-Test (CORRCOEF function) in MATLAB R2016a (The MathWorks, Inc., Natick, Massachusetts, United States) for each pixel [33], and it was tested at significance level threshold of P value = 0.05 for this study.

2.3.3. Ecosystem Water Use Efficiency and Ecosystem Resilience

The eWUE was extracted from available daily global GPP and annual ET datasets, generated using MOD17 algorithm. The eight-day GPP product was processed by the MOD17 algorithm considered vegetation productivity which is directly related to the absorbed solar energy. The algorithm estimated the fraction of photosynthetically active radiation (FPAR) multiplied from MOD15 and daily PAR at pixel level from GMAO NASA

with a set of biome-specific radiation use efficiency (ϵ) to produce the daily absorbed photosynthetically active radiation (APAR) and predict the daily GPP [42]. The daily GPP were aggregated to form the annual GPP, and the mean annual GPP values were evaluated in comparison to GPPEC from global FLUXCOM observations, Carbon fluxes developed based on model tree ensemble (<https://www.bgc-jena.mpg.de/geodb/projects/Data.php>) using R2 coefficient and RMSE error. Likewise, the mean annual ET datasets were compared with the monthly evapotranspiration product of the USGS early warning system for the African continent (<https://earlywarning.usgs.gov/fews/product/66>), which was averaged as annual ET (2000–2014) for the Horn of Africa. Finally, we generated the annual ecosystem water use efficiency (eWUE) from the ratio of average annual MODIS GPP to the average annual ET for the last 15 years.

The trend of the eWUE and drought patterns from the SPEI dataset were detected using a linear regression model similar to the MODIS NDVI trend method (Section 2.3.1). The eWUE trend result was aggregated into different land cover types (CCI-LC) and Agro-ecological zones of the area of interest. Finally, the ecosystem resilience to drought was calculated using the dimensionless ecosystem resilience index (eRD) from the ratio of mean values of multi-annual eWUE to the annual eWUE of the driest year as initially defined by Sharma and Goyal [43] and further applied in other studies [44,45]. The driest year (2009) of high drought severity in the Horn of Africa was identified from the spatial and temporal patterns of the high-resolution annual SPEI images, this was also checked and matched with the EM-DAT record of drought [46]. The eRD was finally classified into four major classes as shown in Table 1.

Table 1. Ecosystem resilience to drought using dimensionless ecosystem Resilience Index (eRD).

No.	Resilience Status	Range
1	Resilient	≥ 1 eRD
2	Slightly Non-Resilient	$0.9 \leq \text{eRD} < 1$
3	Moderately Non-Resilient	$0.8 \leq \text{eRD} < 0.9$
4	Non-Resilient	$\text{eRD} < 0.8$

3. Results

3.1. Annual and Seasonal Vegetation Trends (2000–2019)

A pixel-based trend analysis was performed for the annual and seasonal NDVI trends for the last two decades to properly understand the vegetation dynamics to the recent climate variability and changes over the Horn of Africa. Figure 3a represents the annual mean MODIS NDVI trend and the slope increased at an average rate of 6.2×10^{-4} per year during the period 2000–2019; 1, 205, 709 km² of the area (51.7%) represent an increasing trend ($p < 0.05$). Similarly, the MODIS NDVI trends in the Horn of Africa increased at an average rate of 3.5×10^{-4} , 2.34×10^{-4} , 2.01×10^{-4} , 7.7×10^{-4} per year from March to May (53.1% of the pixels), from June to August (56.2%), from September to November (56.9%), and from December to February (50.8%) seasons (Figure 3b–e), respectively. The vegetation change trends did not show considerable variations among the different seasons of the Horn of Africa.

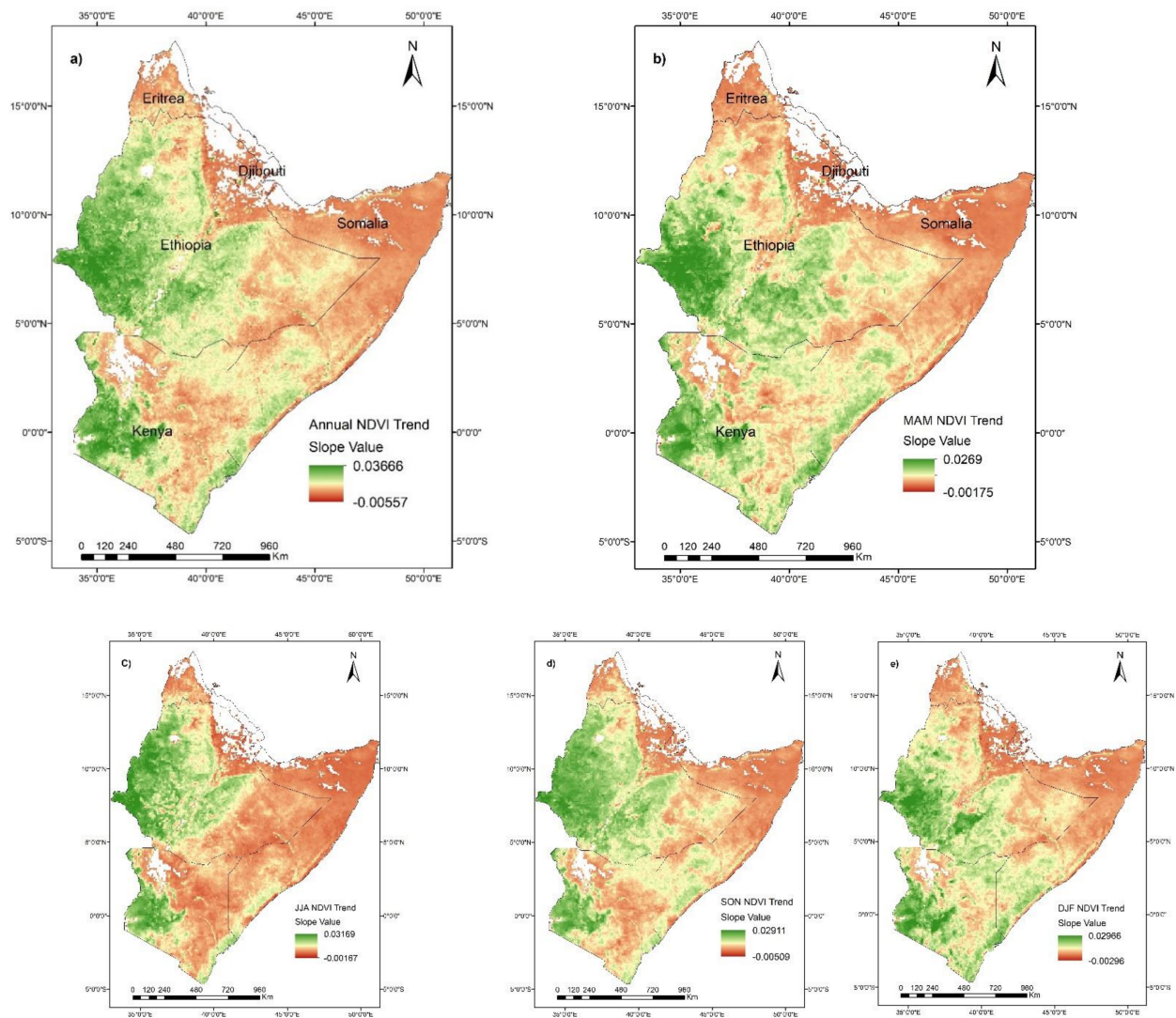


Figure 3. NDVI trends during 2000–2019 in the Horn of Africa. (a) Annual mean and (b–e) seasonal mean trends.

Even though the annual mean NDVI trend slightly showed an increasing trend, yet the trend differs in the area depending on the type of agroecological zones and land cover types. For instance, the maximum positive NDVI trends were common in western parts of Ethiopia and Kenya, while negative NDVI trends were exhibited in large parts of Somalia, Djibouti, and Eritrea (Figure 3). Figure 4 shows the integration of the mean annual NDVI trend with ESA land cover and agroecological zones. The forest and cropland land covers showed the largest increase in the annual mean NDVI trend (Figure 4a), while the smallest trend change was observed in grassland cover during the past two decades apart from the sparse vegetation and the barren land as most of the barren land covers are masked out in the analysis.

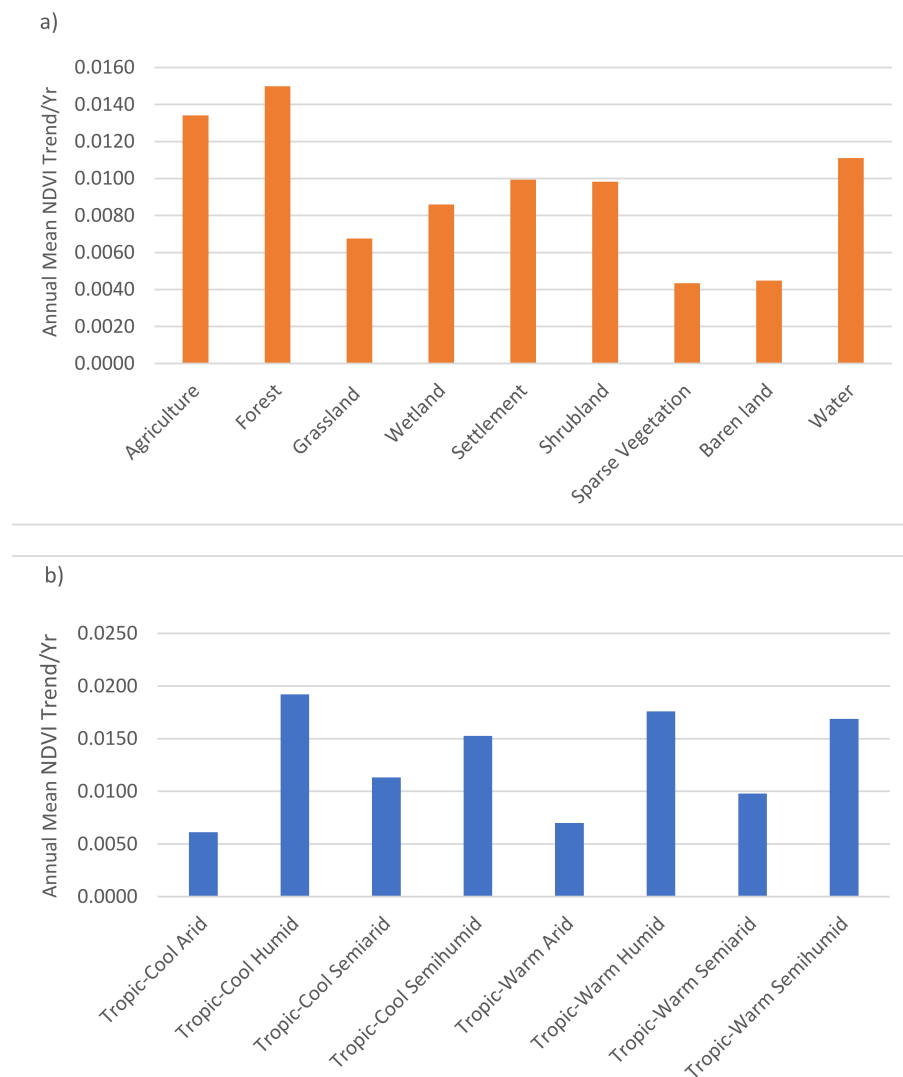


Figure 4. Annual mean NDVI trends per land cover type (a) and per agroecological zones (b) over the Horn of Africa during 2000–2019.

We also carried out zonal statistics of the annual mean NDVI trend for the agroecological zone (Figure 4b). The tropic-cool humid agroecological zones comprised the highest increasing NDVI trend, whereas the tropic-cool arid characterized the lowest increasing annual mean NDVI trend as illustrated in Figure 4b. The humidity and aridity factors played key roles in the spatial distribution and trend of the vegetation change in the region. All the seasons in the Horn of Africa showed similar patterns like the annual mean NDVI trend over different agroecological zones and land cover types, yet the highest increasing trend and variation was detected in the season from September to November, even for the sparsely vegetated land cover and arid zones.

3.2. Correlation Analysis between Vegetation Change and Climate Variables

To have a general view and to understand the spatial relationship, first, a Pearson correlation coefficient (PCC) analysis was run based on mean annual values of NDVI, Precipitation and LST (2000–2019). Figure 5 shows the PCC for mean annual NDVI, precipitation and land surface temperature (LST). The pairwise plots in the graph indicate the correlation pattern as positive or negative (orientation of the plots). The first subplot (Figure 5) demonstrates a strong and positive PCC between annual mean NDVI and annual total precipitation ($r = 0.88$). The second subplot shows a strong and negative correlation

between annual NDVI and LST ($r = -0.84$). The third subplot illustrates the relation between annual total precipitation and annual mean LST ($r = -0.82$). Thus, vegetation dynamics was strongly associated with precipitation and land surface temperature.

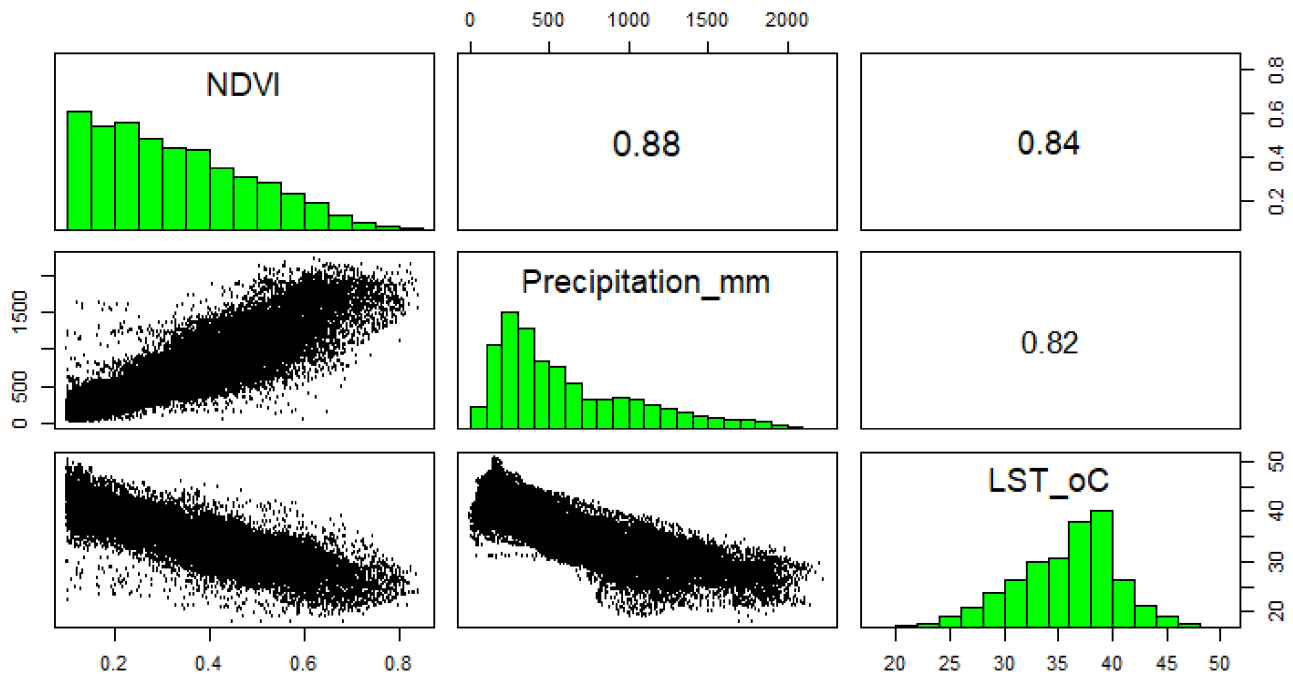


Figure 5. Pearson correlation coefficient (PCC) based on mean annual values of NDVI, precipitation, and LST during 2000–2019 in the Horn of Africa.

There is about 87.6% (1,728,738 km²) of the study area showing a strong and negative correlation between annual mean NDVI and LST (Figure 6a) of which 39.52% (683,197 km²) is statistically significant at $p < 0.05$. Based on zonal statistics, the correlation between NDVI and LST was the strongest and negative in Kenya, while the correlation was only positive in Djibouti. Similarly, based on agroecological zones, the correlation between NDVI and LST was the most significantly and negatively correlated in the tropical warm-subhumid zone, and the weakest negative correlation was observed in the tropical cool-humid zone.

About 93.1% (1,848,823 km²) of the study area is also showing a strong and positive correlation between annual mean NDVI and annual total precipitation during the last two decades (Figure 6b) of which 28.85% (533,385 km²) is significant. The correlation between NDVI and precipitation was the strongest in Kenya and Eritrea, while it was the lowest in Djibouti. Likewise, the correlation between NDVI and precipitation was the most positively correlated in the tropical cool-arid zone, and the weakest positive correlation was observed in the tropical cool-humid zone.

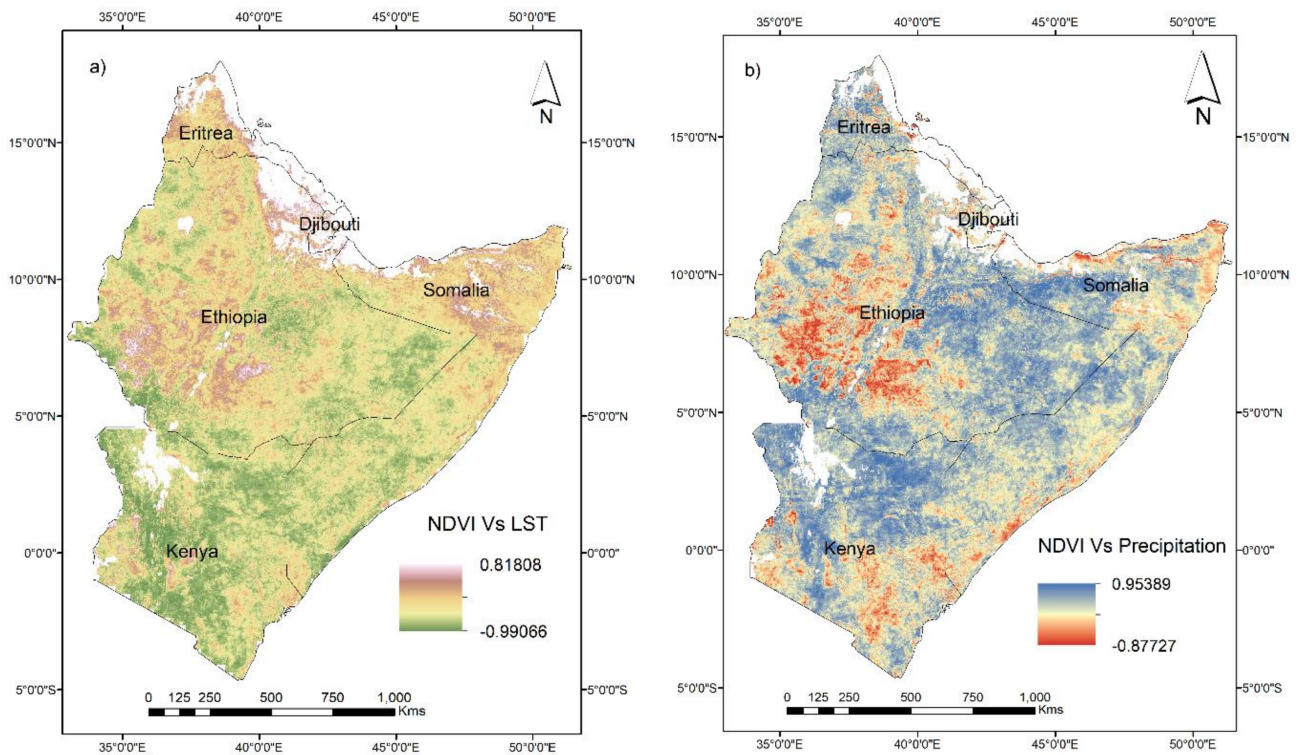


Figure 6. (a) Pixel-based correlations of annual mean NDVI versus land surface temperature (a) and versus precipitation (b) over the Horn of Africa during 2000–2019.

3.3. Annual Ecosystem Water Use Efficiency, Trends and Drivers

3.3.1. Spatial Distributions of Mean Annual GPP, ET, and eWUE across the Horn of Africa

The spatial distribution maps for mean annual GPP, ET and eWUE across the Horn of Africa during 2000–2014 can be observed in Figure 7. The highest values of GPP and ET were concentrated in southwestern highlands of Ethiopia and Kenya with shallow extents in coastal area of Kenya and Southern Somalia. The accuracy of the mean annual GPP was evaluated using GPPEC from Global FLUXCOM observations and obtained R^2 and RMSE values of 0.78 and 5.4 g C m^{-2} , respectively. The mean annual MODIS ET values was also compared to the annual averaged ET from the monthly evapotranspiration product of USGS early warning system for the study area and scored R^2 value of 0.76. Some areas in the eastern lowlands had low values of GPP and ET as these areas received low annual precipitation and represented areas of sparse vegetation.

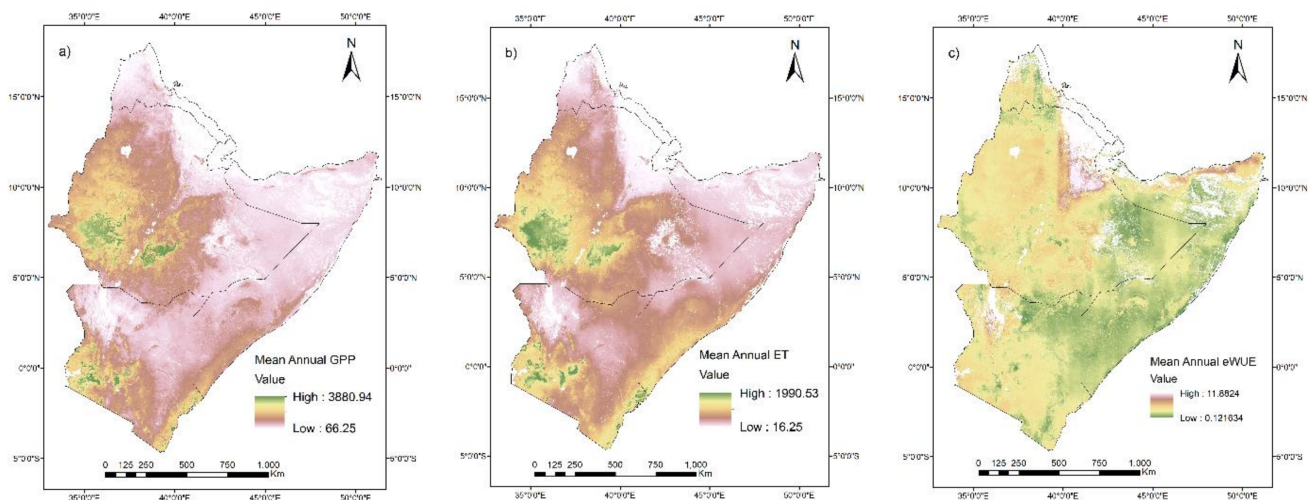


Figure 7. (a) Mean annual distributions of GPP (a, in g C m^{-2}), of ET (b, in mm) and of eWUE (c, in $\text{g C kg}^{-1} \text{H}_2\text{O}$) during 2000–2014 in the Horn of Africa.

The mean annual eWUE in the Horn of Africa was $1.58 \text{ g C kg}^{-1} \text{H}_2\text{O}$ having large spatial variability with a standard deviation of 0.51. The highest mean annual eWUE were observed in large parts of Ethiopia followed by Eritrea, while Somalia and Djibouti had the lowest mean annual eWUE. We also extracted zonal statistics based on the ESA land cover types (Figure 2). The highest mean annual eWUE were found in the cropland and forest land cover types, and the least mean annual eWUE values were observed in the sparse vegetation and wetland areas. The shrubland which is the most dominant land cover (38.9%) in the Horn of Africa had relatively lower mean annual eWUE, whereas the grassland and sparsely vegetated lands had higher standard deviations and eWUE values.

3.3.2. Water Use Efficiency and Drought Trends, and Correlation with Climate Variables

Figure 8a shows the annual eWUE linear trend during 2000–2014. Overall, the slope of the WUE increased at an average rate of $9.6 \times 10^{-3} \text{ g C kg}^{-1} \text{H}_2\text{O y}^{-1}$. The annual eWUE trend increased significantly at a higher rate in larger parts of Kenya and Ethiopia. On the contrary, the annual eWUE showed a decreasing trend in Eritrea especially in southwestern parts of the country, and the average increasing eWUE trend was the smallest in the country ($-3.7 \times 10^{-3} \text{ g C kg}^{-1} \text{H}_2\text{O y}^{-1}$). The annual eWUE based on agroecological zones showed the maximum increasing trend in the tropical warm-semiarid zone, however, all other agroecological zones showed a more or less similar increasing trend. Likewise, the annual eWUE showed the highest increasing trend in the grassland from all other land cover types.

We also evaluated SPEI-12 and generated trend map for the last 15 years to assess the degree of drought severity in the Horn of Africa and associated it with the ecosystem water use efficiency patterns. Figure 8b shows the SPEI-12 trend during 2000–2015. The temporal drought trend using Mann–Kendal showed an overall increasing trend with the mean slope value of 0.05867 y^{-1} . The most severe drought was observed in the year 2009 with a minimum of -1.7 SPEI scale of the annually averaged values. There is about 19.4% ($404,787 \text{ km}^2$) of the study area showing a decreasing SPEI-12 trend. This indicates the severity of the drought had slightly increased in recent years as the decreasing trend in the SPEI time scale corresponds to the increasing drought pattern especially in the northern latitudes between 10° N and 18° N .

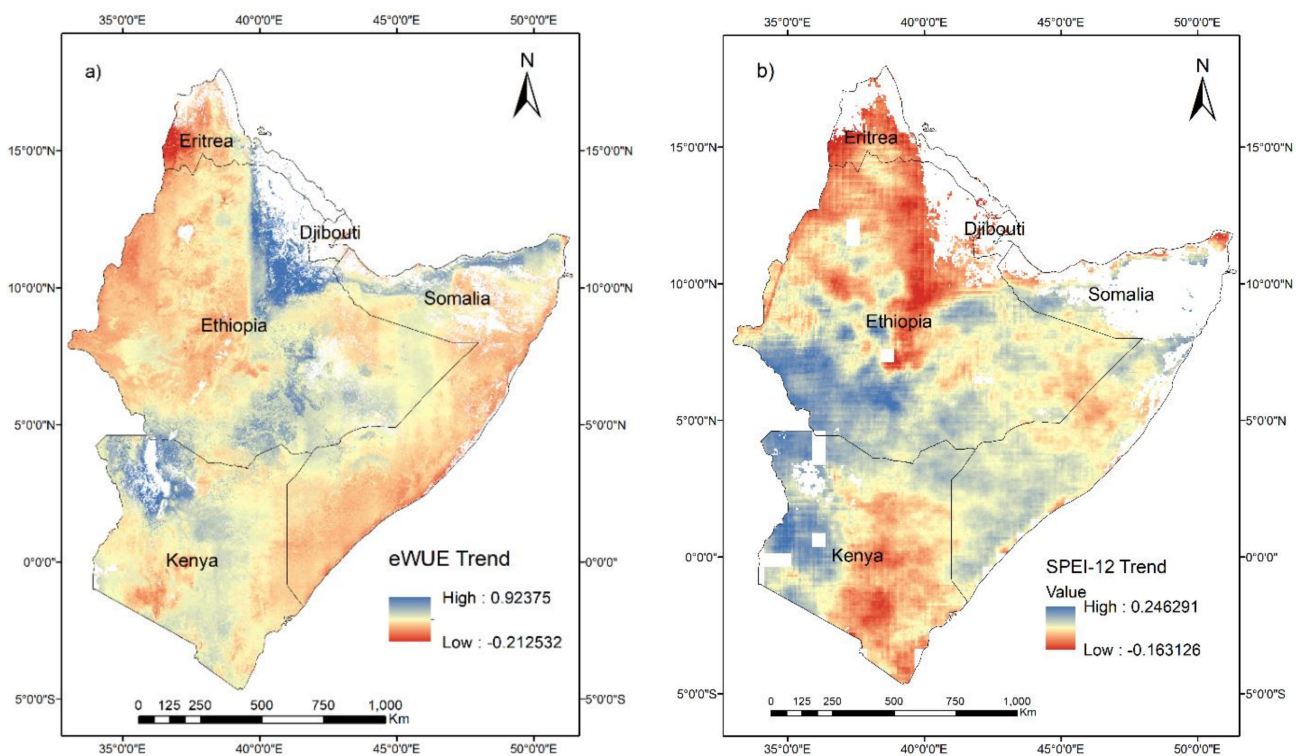


Figure 8. (a) Ecosystem water use efficiency annual trend; (b) drought trend using SPEI-12 in the Horn of Africa during 2000–2019.

Moreover, we assessed the pixel-based correlation coefficient to understand the relationship of the annual eWUE with climatic drivers (LST and Precipitation) and drought (SPEI-12) during the period 2000–2014. About 42.6% (940,015 km²) of the area in Figure 9a shows a negative correlation between annual eWUE and mean LST of which 3.26% (30,645 km²) is statistically significant ($P < 0.05$). There is also about 49.28% (1,095,745 km²) area in Figure 9b showing a strong and positive correlation between annual eWUE and total annual precipitation of which 4.1% (44,926 km²) is significant. Similarly, about 36.54% (723,523 km²) of the study area demonstrates a negative correlation between annual eWUE and SPEI-12 with only 1.3% significant pixels (9406 km²). The correlation of eWUE was the most positively correlated with SPEI-12 in the tropical cool-arid zone, and it had a strong and negative correlation in the Tropical warm-subhumid zone.

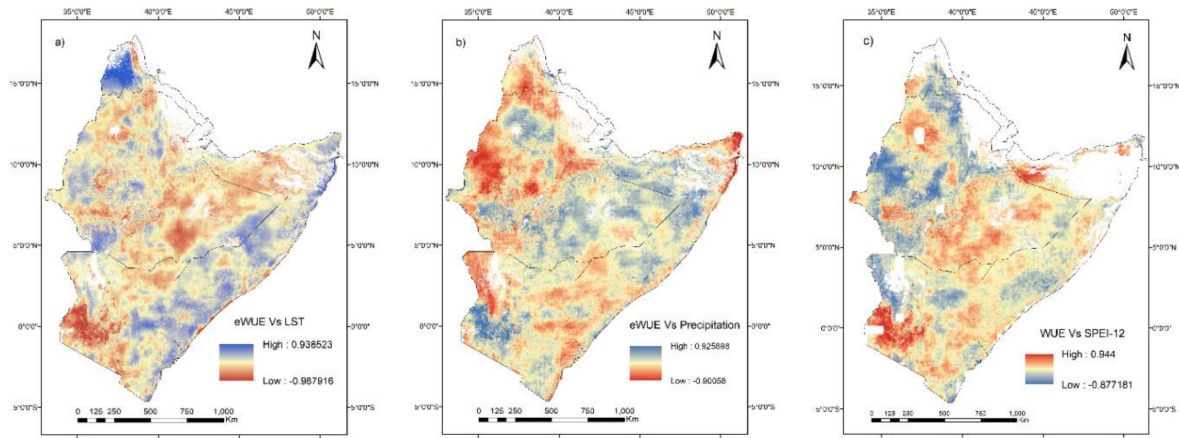


Figure 9. The correlation coefficient of annual eWUE versus mean annual land surface temperature (a), total annual precipitation (b), and SPEI-12 during 2000–2014 in the Horn of Africa (c).

3.3.3. Ecosystem Resilience to Drought Conditions

The mean annual eWUE and annual eWUE values in the most severe drought year were used to determine the ecosystem resilience to drought disturbance, and the results are presented in Figure 10, which shows the ecosystem resilience (Rd) to drought during 2000–2014. Overall, 54.9% of the study area (1,198,476 km²) was found to be resilient to drought: most of the resilient ecosystems were distributed in central highlands of Eritrea, south-eastern Ethiopia, Northeastern Kenya, and large parts of Somalia. In contrast, 32.6%, 9.6%, and 2.8% of the region were non-resilient, moderately non-resilient, and slightly non-resilient, respectively. The severely non-resilient ecosystems were mainly found in south-eastern parts of Kenya, Southwestern Eritrea, and areas near the triple junction of Ethiopia, Djibouti, and Somalia.

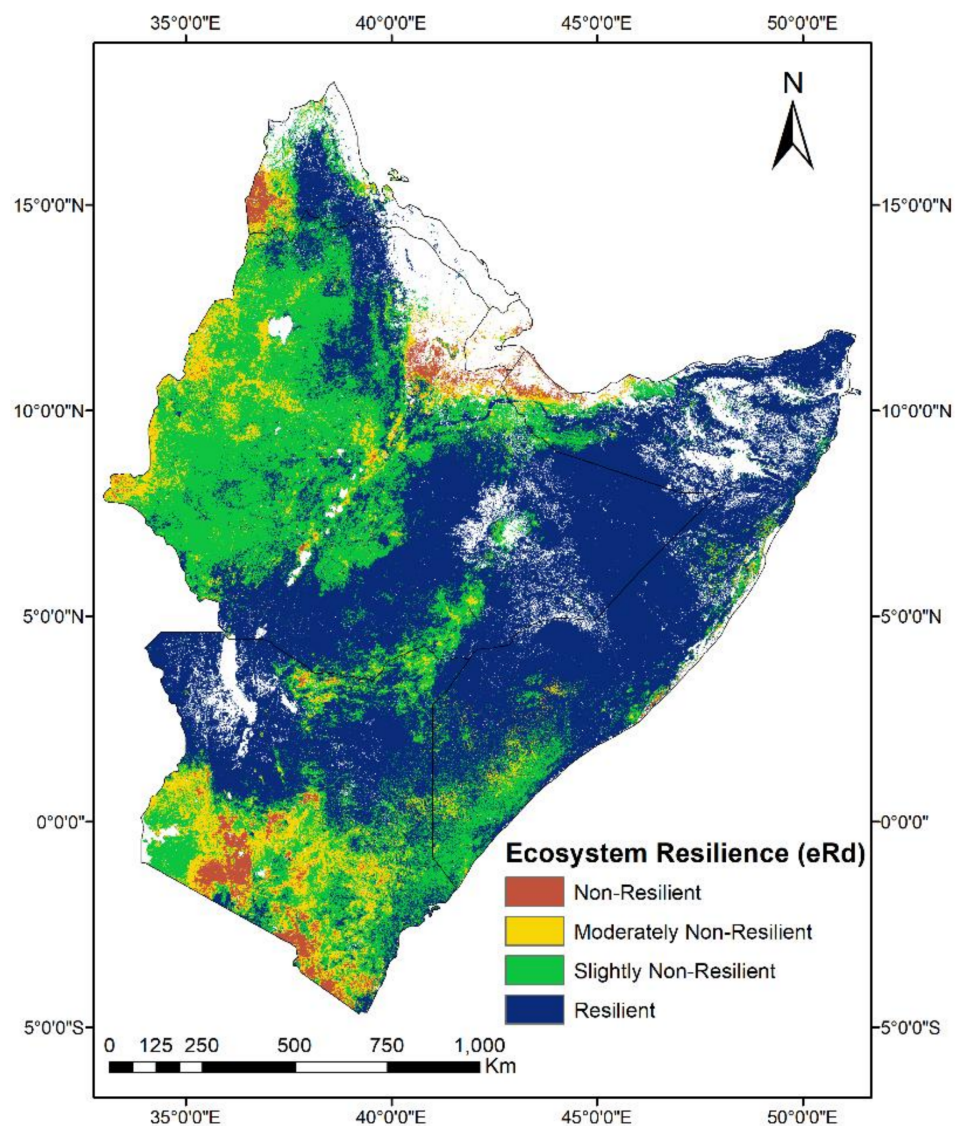


Figure 10. Ecosystem resilience (eRd) to drought based on eWUE in the Horn of Africa (2000–2014).

We also integrated the final ecosystem resilience result with different land cover types and agroecological zones of the region. The cropland and wetland were slightly non-resilient to drought with mean eRd values of 0.97 and 0.99, correspondingly. While, grassland and sparse vegetation were relatively the most resilient to drought with mean eRd values of 1.12 and 1.1, respectively. Likewise, the tropic warm-humid with mean

($R_d = 0.92$) and the tropic cool-humid ($eR_d = 0.94$) were slightly non-resilient to drought, whereas the tropic warm-arid ($eR_d = 1.13$) and cool-arid agroecological zones showed relatively the highest resilience to drought disturbance in the region.

4. Discussion

4.1. Assessment of MODIS NDVI Trends and Climate Variables

The pixel-based results of the annual and seasonal trends of vegetation dynamics in the Horn of Africa (Figure 3) revealed that there were areas of vegetation change in the last two decades. There were some changes in MODIS NDVI trend towards an overall positive trend, however, 49.3% of the pixels in the region experienced a decreasing NDVI trend mainly because of the increasing climate variability, recurrent drought and vegetation degradation. Kalisa et al. [24] identified that the NDVI trend was increasing in 47% of the pixels and decreasing in 49% of the pixels across East Africa during 1998–2015. Our result showed a slight improvement in the average annual NDVI trend in comparison to Ghebregabher et al. [47] which concluded the average NDVI in the Horn of Africa slowly decreased from 1998 to 2013, this could be due to the difference in the study duration as we included some recent years (until 2019) in the analysis, and the break-in 1998 was another factor to bring slight variation in the trend across the region with fluctuations in the intensity of precipitation [22].

The weakest NDVI trends in the Horn of Africa were observed in the grassland cover and the tropic-cool/arid zones in the last two decades. The grassland in the arid lands was most affected because of the increasing aridity and recurrent drought with climate variability in the region, and the grassland and shrubland covers are more sensitive to the impacts of climate change [1,25,33]. The highest vegetation increase was observed in from September to November season, the time lag effect of the short rainy season from June to August in Ethiopia, Eritrea and Somalia, and the effect of ENSO might be large on the NDVI variations [24].

The main climatic drivers for the vegetation changes in the Horn of Africa showed that the LST was negatively and significantly correlated with NDVI, while precipitation was positively and significantly correlated in the past 20 years (Figure 6). The results match with the findings of Ghebregabher et al. [25] to the reverse proportional and significant correlation between NDVI and temperature (LST in our case) which could be attributed to global warming, average net warming and non-radiative processes [28], and the correlation showed the highest significance in the tropical warm-subhumid zone. On the other hand, they reported there was insignificant proportional relationship between NDVI and Precipitation, however, our result reveals that the response of NDVI to rainfall was significant in the region as the intensity of precipitation and fluctuation has been increasing [1]. The response of vegetation to precipitation was poor in the tropical cool-humid zone, this can be associated basically to the influence of 'saturation' of the NDVI which reacted slowly through time even with the increase in the intensity and fluctuation of rainfall in humid areas [48,49].

4.2. Water Use Efficiency Variations and Drivers

The multi-annual eWUE estimates (Figure 7c) showed high temporal and spatial variation across the Horn of Africa which could be influenced by different factors including climate, drought, vegetation cover and physical characteristics of the region [5]. For instance, the highest eWUE in Ethiopia might be due to the presence of forests, increasing temperature and availability of large croplands in the country. The lowest mean annual eWUE in the shrublands was observed probably due to its low vegetation productivity relative to the other land cover types in the region. The annual eWUE showed an overall increasing trend in the Horn of Africa, and the result matches with the findings of [21] who concluded an overall increased mean and trend of eWUE for different land cover types in Africa. However, our result showed the most increasing trend for the grassland rather than the forest land cover which could be due to differences in the spatial extent, GPP and ET

data sources and their spatial resolutions. The observed increasing trend of eWUE in the grassland might be attributed to the growing intensity and fluctuations of precipitation, water stress and drought conditions. Several studies indicated that different vegetation types tend to increase in eWUE due to water stress conditions [45,50].

The main driving forces behind the eWUE spatial and temporal variations in the Horn of Africa can be understood from the correlation of eWUE to LST, precipitation, and SPEI-12 (Figure 9). It can be concluded that an increasing precipitation intensity had the most significant influence on the eWUE variations in the region as the significance percentage of the correlation between eWUE and precipitation was the highest compared to the influences of LST and SPEI-12. The precipitation and eWUE had the most positive and significant correlation for the Shrubland and tropic cool-humid ecosystems, while there were negative and significant correlations for the grassland and tropic warm-subhumid ecosystems. The negative correlation between eWUE and precipitation was common in the semi-arid regions of Kenya, Ethiopia, and Eritrea with grassland cover in the region, this could be largely due to different rates of ET and GPP in the last two decades.

A recent study by Gebremeskel et al. [51] confirmed that there was a significant increase in the drought frequency, duration and severity across the Greater Horn of Africa. Especially, a higher magnitude of the drought was reported in Somalia, Ethiopia, and Kenya. The effect of the drought could be immense on different biomes. We specifically investigated the drought in the region using SPEI-12 to understand the recent drought trend (Figure 8b), and its relationship with eWUE (Figure 9c). In large part of the Horn of Africa, the SPEI-12 drought trend showed an increasing trend, however, there were specific areas which showed insignificant decreasing drought trend. Similar non-significant decreasing trends were also identified by Gebremeskel Haile et al., [51] and Mpelasoka et al., [52] in the Greater of Horn of Africa which covers six other countries apart from our study area. This indicates that the severity of the drought had slightly increased in the past two decades. The decreasing trend in the SPEI time scale corresponds to the increasing hydrological drought especially in the northern latitudes between 10° N and 18° N and below the equator where the location and climatic factors had contributed the pattern. The most significant negative correlation between eWUE and SPEI-12 was observed for the shrubland and other biomes in the tropical warm-subhumid zone. The main reason could be probably the decrease in GPP was higher than for ET which led to an increase in eWUE during drought conditions as highlighted by Huang et al. [50].

4.3. Implications of Vegetation Dynamics and Ecosystem Resilience to Drought

The results of the pixel-based annual and seasonal trends of vegetation dynamics in the Horn of Africa showed areas of increasing and decreasing vegetation change, while there were weak NDVI trends for the grassland cover specifically in the arid lands. Similarly, the eWUE analysis based on the GPP and ET measurements revealed that there was an overall increasing trend of annual eWUE with the trend increased most in the grassland cover showing higher efficiency under water stress and drought conditions. The implications of the results indicate the climate variability and climate change have affected the different biomes of the ecosystems; the grassland and shrublands were the most vulnerable in the Horn of Africa. Niang et al. [1] confirmed in the IPCC 2014 report that the impacts of climate change are more visible with occurrences of drought, water scarcity, and increasing threats in human health and biodiversity problems upon which Africa is the most vulnerable continent of the world. The drivers behind the NDVI change and eWUE variations showed that the key controlling factor was the intensity and fluctuation of precipitation in the region (Figures 6 and 9), however, the effect and resilience of the whole ecosystem could be caused by multiple factors. The drought was a secondary factor which affected the ecosystem and the response of each biome differs from place to place.

The Horn of Africa has been exposed to recurrent drought conditions. The final map of ecosystem resilience (Figure 10) showed that 54.9% was resilient to drought disturbance, while 32.6% was completely non-resilient. This is mostly in agreement with the recent study

on ecohydrological resilience to ecosystem shifts over the African continent [21]. However, our result showed that cropland and wetland were slightly non-resilient ecosystems to drought condition rather than the savannahs and barren lands. The ecosystem resilience to drought reveals that the warm-humid and cool-humid agroecological zones were slightly non-resilient to the most severe drought conditions; this indicates the vulnerability of these ecosystems to the warming trends and impacts of climate change in the region. The delimitation of non-resilient areas could be helpful to target local regions, and enhance their resilience to drought and minimize the environmental impacts from climate change; thereby can contribute to the ecosystem-centered drought protection, adaptation, and alleviation measures at a regional level. This action would further strengthen the management of water resources and terrestrial ecosystems in the region as the response of eWUE to drought conditions and the changing climate in each biome differs from place to place. The overall implication of the vegetation dynamics and productivity with variations in eWUE provides useful spatial and temporal information for policy and decision-makers. This can play a vital role in rangeland management, ranching decisions and strategies, vegetation degradation protection and management, drought and climate change mitigation measures at national and regional levels.

5. Conclusions

In this study, the pixel-based results of the annual and seasonal trends of MODIS NDVI showed there were areas of increasing and decreasing vegetation change in the last two decades across the Horn of Africa. There was an overall positive NDVI trend in the region, while 49.3% (1,149,713 km²) of the area experienced a decreasing NDVI trend. The effects of climate variability could be evidenced with NDVI as an indicator of the inter-annual variability in the region, and the weakest NDVI trends were observed in the grassland cover and the tropic-cool arid zones. The NDVI was negatively correlated with LST, and it was positively correlated with the precipitation variability in the Horn of Africa. In the study area, 39.52% (683,197 km²) had a significant negative correlation between NDVI and LST, whereas 28.85% (533,385 km²) was significantly correlated with precipitation. The response of vegetation to precipitation and LST was specifically poor in the Tropic cool-humid zone which reflected the saturation impact of the biomes in the region. We further investigated the water use efficiency and ecosystem resilience in the region using MODIS GPP and ET to drought and climate drivers during 2000–2014. The trend of eWUE showed an overall increasing trend with a large impact on the grassland cover mainly due to its higher efficiency under water stress and drought conditions. Based on multi-annual pixel-based correlation analysis, the precipitation had the most significant effect on the eWUE variations in the Horn of Africa in comparison to the influences of LST and SPEI-12 drivers. The final ecosystem resilience to drought showed 54.9% of the region was resilient to drought disturbance, while 32.6% was completely non-resilient. The ecosystems in the humid agro-ecological zones specifically the cropland and wetland were the slightly non-resilient to severe drought conditions which need special attention in the regional ecosystem planning and management. Future research works should work more on the impacts of multiple drivers and integrate climate change scenarios.

Author Contributions: Conceptualization: B.C. and S.M.; data curation: S.M., D.C., and L.G.; formal analysis: S.M., B.C., P.P., and L.G.; funding acquisition: B.C.; investigation: S.M. and P.P.; methodology: S.M., B.C., X.S., and D.C.; project administration: B.C.; resources: B.C. and S.M.; software: S.M., H.Z., and L.G.; supervision: B.C., and P.P.; validation: B.C., P.P., S.S., A.K., and X.S.; visualization: S.M., H.Z., and D.C.; writing—original draft: S.M., P.P., B.C., and M.G.; writing—review and editing: B.C., P.P., M.G., A.K., S.S., H.Z., and X.S. All authors have read and agreed to the published version of the manuscript.

Funding: This research work was supported by National Key R&D Program of China (grant nos. 2018YFA0606001, 2017YFA0604301, and 2017YFA0604302), the research grants 41771114 and 41977404 funded by the National Natural Science Foundation of China, and the research grant O88RA901YA

funded by the State Key Laboratory of Resources and Environment Information System. The first author was sponsored by the Chinese Government Scholarship for his PhD study.

Data Availability Statement: In this study, publicly available datasets were accessed and analyzed. Time series images of MODIS NDVI Terra 16-day, Land Surface Temperature of MODIS Terra 8-day, and CHIRPS daily gridded precipitation datasets can be accessed here (accessed on 26 October 2020): [<https://app.climateengine.org/climateEngine>]. The Global GPP and ET images as annual MOD17A3 and MOD16A3 products are available: http://files.ntsug.umt.edu/data/NTSG_Products/ (accessed on 21 December). The SPEI-12 month's dataset (0.05°) for Africa from CEDA Archive of the Natural Environment Research Council's Data Repository can be found: <https://catalogue.ceda.ac.uk/> (accessed on 15 November 2020).

Acknowledgments: Authors acknowledge the MODIS of the NASA and Numerical Terra-dynamic Simulation Group who let us to access high resolution time series images of NDVI, Land Surface Temperature, global daily GPP, and ET products. We thank the Climate Hazards Group for providing the daily CHIRPS precipitation data available through Climate Engine and Google Earth Engine. Authors also thank the CEDA Archive of the Natural Environment Research Council's Data Repository for providing the high resolution SPEI dataset for Africa. PP would like to acknowledge ESSA (Earth observation and environmental sensing for climate-smart sustainable agropastoral ecosystem transformation in East Africa) funded under DeSIRA program of the European Commission (contract FOOD/2020/418-13) for a consortium led by University of Helsinki, and SMARTLAND project (Environmental sensing of ecosystem services for developing a climate-smart landscape framework to improve food security in East Africa) funded by the Academy of Finland (318645).

Conflicts of Interest: The authors declare no conflict of interest.

References

- Niang, I.; Ruppel, O.C.; Abdrabo, M.A.; Essel, A.C.; Lennard, J.; Padgham, P.U. *Climate Change 2014—Impacts, Adaptation and Vulnerability: Regional Aspects*; Cambridge University Press: Cambridge, MA, USA, 2014; pp. 1199–1265.
- Ayana, E.K.; Ceccato, P.; Fisher, J.R.B.; DeFries, R. Examining the relationship between environmental factors and conflict in pastoralist areas of East Africa. *Sci. Total Environ.* **2016**, *557–558*, 601–611. [[CrossRef](#)] [[PubMed](#)]
- Daron, J. Regional Climate Messages for East Africa, Scientific report from the CARIAS Adaptation at Scale in Semi-Arid Regions (ASSAR) Project. 2014. Available online: www.assar.uct.ac.za/sites/default/files/image_tool/images/138/RDS_reports/climate_messages/SouthernAfricaClimateMessages-Version1-RegionalLevel.pdf (accessed on 26 October 2020).
- Gemeda, D.O.; Sima, A.D. The impacts of climate change on African continent and the way forward. *JENE* **2015**, *7*, 256–262.
- Abera, T.A.; Heiskanen, J.; Pellikka, P.; Maeda, E.E. Rainfall–vegetation interaction regulates temperature anomalies during extreme dry events in the Horn of Africa. *Glob. Planet. Change* **2018**, *167*, 35–45. [[CrossRef](#)]
- Measho, S.; Chen, B.; Pellikka, P.; Trisurat, Y.; Guo, L.; Sun, S.; Zhang, H. Land Use/Land Cover Changes and Associated Impacts on Water Yield Availability and Variations in the Mereb-Gash River Basin in the Horn of Africa. *J. Geophys. Res. Biogeosci.* **2020**, *125*, 1–16. [[CrossRef](#)]
- Stévant, T.; Dauby, G.; Lowry, P.; Blach-Overgaard, A.; Droissart, V.; Harris, D.J.; Mackinder, A.B.; Schatz, G.E.; Sonké, B.; Sosef, M.S.M.; et al. A third of the tropical African flora is potentially threatened with extinction. *Sci. Adv.* **2019**, *5*, 1–13. [[CrossRef](#)]
- Tolessa, T.; Senbeta, F.; Kidane, M. The impact of land use/land cover change on ecosystem services in the central highlands of Ethiopia. *Ecosyst. Serv.* **2017**, *23*, 47–54. [[CrossRef](#)]
- Pellikka, P.K.E.; Heikinheimo, V.; Hietanen, J.; Schäfer, E.; Siljander, M.; Heiskanen, J. Impact of land cover change on aboveground carbon stocks in Afromontane landscape in Kenya. *Appl. Geogr.* **2018**, *94*, 178–189. [[CrossRef](#)]
- Abera, T.A.; Heiskanen, J.; Pellikka, P.K.E.; Adhikari, H.; Maeda, E.E. Climatic impacts of bushland to cropland conversion in Eastern Africa. *Sci. Total Environ.* **2020**, *717*, 137255. [[CrossRef](#)] [[PubMed](#)]
- Midgley, G.F.; Bond, W.J. Future of African terrestrial biodiversity and ecosystems under anthropogenic climate change. *Nat. Clim. Chang.* **2015**, *5*, 823–829. [[CrossRef](#)]
- Roerink, G.J.; Menenti, M.; Soepboer, W.; Su, Z. Assessment of climate impact on vegetation dynamics by using remote sensing. *Phys. Chem. Earth* **2003**, *28*, 103–109. [[CrossRef](#)]
- Zhang, X.; Friedl, M.A.; Schaaf, C.B.; Strahler, A.H.; Hodges, J.C.F.; Gao, F.; Reed, B.C.; Huete, A. Monitoring vegetation phenology using MODIS. *Remote Sens. Environ.* **2003**, *84*, 471–475. [[CrossRef](#)]
- Bao, G.; Qin, Z.; Bao, Y.; Zhou, Y.; Li, W.; Sanjiv, A. NDVI-based long-term vegetation dynamics and its response to climatic change in the Mongolian plateau. *Remote Sens.* **2014**, *6*, 8337–8358. [[CrossRef](#)]
- Aalto, I.; Maeda, E.E.; Heiskanen, J.; Pellikka, P. Assessing the cooling effect of tree canopies in an intensively modified Afromontane landscape. 2021; unpublished work.
- Xie, B.; Jia, X.; Qin, Z.; Shen, J.; Chang, Q. Vegetation dynamics and climate change on the Loess Plateau, China: 1982–2011. *Reg. Environ. Chang.* **2015**, *16*, 1583–1594. [[CrossRef](#)]

17. Forkel, M.; Carvalhais, N.; Verbesselt, J.; Mahecha, M.D.; Neigh, C.S.R.; Reichstein, M. Trend Change detection in NDVI time series: Effects of inter-annual variability and methodology. *Remote Sens.* **2013**, *5*, 2113–2144. [[CrossRef](#)]
18. Sun, S.; Song, Z.; Wu, X.; Wang, T.; Wu, Y.; Du, W.; Che, T.; Huang, C.; Zhang, X.; Ping, B.; et al. Spatio-temporal variations in water use efficiency and its drivers in China over the last three decades. *Ecol. Indic.* **2018**, *94*, 292–304. [[CrossRef](#)]
19. Huang, M.; Piao, S.; Zeng, Z.; Peng, S.; Ciais, P.; Cheng, L.; Mao, J.; Poulter, B.; Shi, X.; Yao, Y.; et al. Seasonal responses of terrestrial ecosystem water-use efficiency to climate change. *Glob. Chang. Biol.* **2016**, *22*, 2165–2177. [[CrossRef](#)] [[PubMed](#)]
20. Herrmann, S.M.; Anyamba, A.; Tucker, C.J. Recent trends in vegetation dynamics in the African Sahel and their relationship to climate. *Glob. Environ. Chang.* **2005**, *15*, 394–404. [[CrossRef](#)]
21. Kayiranga, A.; Chen, B.; Trisurat, Y.; Ndayisaba, F.; Sun, S.; Tuankrua, V.; Wang, F.; Karamage, F.; Measho, S.; Nthangeni, W.; et al. Water Use Efficiency-Based Multiscale Assessment of Ecohydrological Resilience to Ecosystem Shifts Over the Continent of Africa During 1992–2015. *J. Geophys. Res. Biogeosci.* **2020**, *125*, 1–19. [[CrossRef](#)]
22. Musau, J.; Patil, S.; Sheffield, J.; Marshall, M. Spatio-temporal vegetation dynamics and relationship with climate over East Africa. *Hydrol. Earth Syst. Sci. Discuss.* **2016**, *19*, 1–30.
23. Pricope, N.G.; Husak, G.; Lopez-Carr, D.; Funk, C.; Michaelsen, J. The climate-population nexus in the East African Horn: Emerging degradation trends in rangeland and pastoral livelihood zones. *Glob. Environ. Chang.* **2013**, *23*, 1525–1541. [[CrossRef](#)]
24. Kalisa, W.; Igbawua, T.; HENCHIRI, M.; Ali, S.; Zhang, S.; Bai, Y.; Zhang, J. Assessment of climate impact on vegetation dynamics over East Africa from 1982 to 2015. *Sci. Rep.* **2019**, *9*, 1–20. [[CrossRef](#)]
25. Ghebregabher, M.G.; Yang, T.; Yang, X.; Eyassu Sereke, T. Assessment of NDVI variations in responses to climate change in the Horn of Africa. *Egypt. J. Remote Sens. Sp. Sci.* **2020**, 1–13. [[CrossRef](#)]
26. Indeje, M.; Semazzi, F.H.M.; Ogallo, L.J. ENSO signals in East African rainfall seasons. *Int. J. Climatol.* **2000**, *20*, 19–46. [[CrossRef](#)]
27. Ogallo, L.J. Relationships between seasonal rainfall in East Africa and the Southern Oscillation. *J. Climatol.* **1988**, *8*, 31–43. [[CrossRef](#)]
28. Abera, T.A.; Heiskanen, J.; Pellikka, P.; Rautiainen, M. Clarifying the role of radiative mechanisms in the spatio-temporal changes of land surface temperature across the Horn of Africa. *Remote Sens. Environ.* **2019**, *221*, 210–224. [[CrossRef](#)]
29. Abera, T.A.; Heiskanen, J.; Pellikka, P.K.E.; Maeda, E.E. Impact of rainfall extremes on energy exchange and surface temperature anomalies across biomes in the Horn of Africa. *Agric. For. Meteorol.* **2020**, *280*, 107779. [[CrossRef](#)]
30. Otieno, V.O.; Anyah, R.O. Effects of land use changes on climate in the Greater Horn of Africa. *Clim. Res.* **2012**, *52*, 77–95. [[CrossRef](#)]
31. Pellikka, P.K.E.; Clark, B.J.F.; Gosa, A.G.; Himberg, N.; Hurskainen, P.; Maeda, E.; Mwang'ombe, J.; Omoro, L.M.A.; Siljander, M. Agricultural Expansion and Its Consequences in the Taita Hills, Kenya. *Dev. Earth Surf. Process.* **2013**, *16*, 165–179.
32. Huntington, J.L.; Hegewisch, K.C.; Daudert, B.; Morton, C.G.; Abatzoglou, J.T.; McEvoy, D.J.; Erickson, T. Climate engine: Cloud computing and visualization of climate and remote sensing data for advanced natural resource monitoring and process understanding. *Bull. Am. Meteorol. Soc.* **2017**, *98*, 2397–2409. [[CrossRef](#)]
33. Measho, S.; Chen, B.; Trisurat, Y.; Pellikka, P.; Guo, L.; Arunyawat, S.; Tuankrua, V.; Ogbazghi, W.; Yemane, T. Spatio-Temporal Analysis of Vegetation Dynamics as a Response to Climate Variability and Drought Patterns in the Semiarid Region, Eritrea. *Remote Sens.* **2019**, *11*, 724. [[CrossRef](#)]
34. Zhao, M.; Running, S.W. Sensitivity of Moderate Resolution Imaging Spectroradiometer (MODIS) terrestrial primary production to the accuracy of meteorological reanalyses. *J. Geophys. Res. Biogeosci.* **2006**, *111*, 1–13. [[CrossRef](#)]
35. Mu, Q.; Zhao, M.; Running, S.W. Improvements to a MODIS global terrestrial evapotranspiration algorithm. *Remote Sens. Environ.* **2011**, *115*, 1781–1800. [[CrossRef](#)]
36. Pérez-Hoyos, A.; Rembold, F.; Kerdiles, H.; Gallego, J. Comparison of global land cover datasets for cropland monitoring. *Remote Sens.* **2017**, *9*, 1118. [[CrossRef](#)]
37. Na-U-Dom, T.; Mo, X.; García, M. Assessing the Climatic Effects on Vegetation Dynamics in the Mekong River Basin. *Environments* **2017**, *4*, 17. [[CrossRef](#)]
38. Osuch, M.; Romanowicz, R.J.; Lawrence, D.; Wong, W.K. Trends in projections of standardized precipitation indices in a future climate in Poland. *Hydrol. Earth Syst. Sci.* **2016**, *20*, 1947–1969. [[CrossRef](#)]
39. Santos, C.A.G.; Brasil Neto, R.M.; da Silva, R.M.; dos Santos, D.C. Innovative approach for geospatial drought severity classification: A case study of Paraíba state, Brazil. *Stoch. Environ. Res. Risk Assess.* **2019**, *33*, 545–562. [[CrossRef](#)]
40. Sun, J.; Qin, X. Precipitation and temperature regulate the seasonal changes of NDVI across the Tibetan Plateau. *Environ. Earth Sci.* **2016**, *75*, 1–9. [[CrossRef](#)]
41. Kang, C.H.; Zhang, Y.; Wang, Z.; Liu, L.; Zhang, H.; Jo, Y. The driving force analysis of NDVI dynamics in the trans-boundary Tumen River Basin between 2000 and 2015. *Sustainability* **2017**, *9*, 2350. [[CrossRef](#)]
42. Running, S.W.; Zhao, M. User's Guide: Daily GPP and Annual NPP (MOD17A2/A3) Products NASA Earth Observing System MODIS Land Algorithm. MODIS Land Team, 2015. Available online: https://www.ntsg.umt.edu/files/modis/MODIS7UsersGuide2015_v3.pdf (accessed on 26 October 2020).
43. Sharma, A.; Goyal, M.K. Assessment of ecosystem resilience to hydroclimatic disturbances in India. *Glob. Chang. Biol.* **2018**, *24*, e432–e441. [[CrossRef](#)] [[PubMed](#)]
44. Guo, L.; Sun, F.; Liu, W.; Zhang, Y.; Wang, H. Response of Ecosystem Water Use Efficiency to Drought over China during 1982–2015: Spatiotemporal Variability and Resilience. *Forests* **2019**, *10*, 958. [[CrossRef](#)]

45. Sharma, A.; Goyal, M.K. District-level assessment of the ecohydrological resilience to hydroclimatic disturbances and its controlling factors in India. *J. Hydrol.* **2018**, *564*, 1048–1057. [[CrossRef](#)]
46. EM-DAT The Emergency Events Database. Available online: <https://www.emdat.be/> (accessed on 18 November 2020).
47. Ghebregabher, M.G.; Yang, T.; Yang, X. Long-term trend of climate change and drought assessment in the Horn of Africa. *Adv. Meteorol.* **2016**, *2016*, 8057641. [[CrossRef](#)]
48. Zhou, J.; Jia, L.; Menenti, M.; van Hoek, M.; Lu, J.; Zheng, C.; Wu, H.; Yuan, X. Characterizing vegetation response to rainfall at multiple temporal scales in the Sahel-Sudano-Guinean region using transfer function analysis. *Remote Sens. Environ.* **2020**, *252*, 112108. [[CrossRef](#)]
49. Davenport, M.L.; Nicholson, S.E. On the relation between rainfall and the Normalized Difference Vegetation Index for diverse vegetation types in East Africa. *Int. J. Remote Sens.* **1993**, *14*, 2369–2389. [[CrossRef](#)]
50. Huang, L.; He, B.; Han, L.; Liu, J.; Wang, H.; Chen, Z. A global examination of the response of ecosystem water-use efficiency to drought based on MODIS data. *Sci. Total Environ.* **2017**, *601–602*, 1097–1107. [[CrossRef](#)] [[PubMed](#)]
51. Gebremeskel Haile, G.; Tang, Q.; Leng, G.; Jia, G.; Wang, J.; Cai, D.; Sun, S.; Baniya, B.; Zhang, Q. Long-term spatiotemporal variation of drought patterns over the Greater Horn of Africa. *Sci. Total Environ.* **2020**, *704*, 135299. [[CrossRef](#)] [[PubMed](#)]
52. Mpelasoka, F.; Awange, J.L.; Zerihun, A. Influence of coupled ocean-atmosphere phenomena on the Greater Horn of Africa droughts and their implications. *Sci. Total Environ.* **2018**, *610–611*, 691–702. [[CrossRef](#)]